National Aviation Academy

International Journal of Transportation Research and Technology

e-ISSN: 3079-6075

DOI: 10.71108/transporttech.vm03is01.01

Research Article

Computational Fluid Dynamics Analysis of the Effect of Trim Angle on Planing Stepped Hulls

Kadir Emrah Erginer[1], Burak Goksu[2], Yasin Furkan Gorgulu*[3]

[1]*Dokuz Eylül University, İzmir, Türkiye*
[2]*Zonguldak Bulent Ecevit University, Zonguldak, Türkiye*
[3]*Eskişehir Osmangazi University, Eskişehir, Türkiye*

Timescale of article

Received: 23 October 2025
Accepted: 19 January 2026
Published: 25 June 2026

Corresponding author

Yasin Furkan Gorgulu
furkan.gorgulu@ogu.edu.tr

Keywords:

Computational fluid dynamics, Froude number, Hydrodynamic resistance, Stepped planing hull, Trim angle

Cite this article as:

Erginer, K. E., Goksu, B., & Gorgulu, Y. F. (2026). Computational Fluid Dynamics Analysis of the Effect of Trim Angle on Planing Stepped Hulls. *International Journal of Transportation Research and Technology*, 3(1), 5-14.
DOI: 10.71108/transporttech.vm03is01.01

Abstract

This study investigates the hydrodynamic influence of trim angle variation on a stepped planing hull using computational fluid dynamics. The analyses were performed in ANSYS Fluent under steady-state RANS conditions with the SST k–ω turbulence model and a Volume of Fluid multiphase setup. Two scenarios were examined: a hull with no trim and a hull trimmed by 1.6°. The computational domain consisted of 3,572,223 elements with high mesh quality metrics, ensuring accurate free-surface and near-wall resolution. Quantitative results show that in the non-trimmed configuration, the maximum flow velocity reached 20.8 $m \cdot s^{-1}$, with an average of 17.0 $m \cdot s^{-1}$ near the hull, while the 1.6° trimmed case exhibited a slightly lower mean surface velocity of 15–16 $m \cdot s^{-1}$ but a more elongated wake. The maximum turbulence kinetic energy decreased from 18 $m^2 \cdot s^{-2}$ to 9.6 $m^2 \cdot s^{-2}$, indicating reduced turbulence intensity and a more stable wake structure. The total drag force decreased dramatically from 22,592.89 N to 3,009.294 N, representing an 86.68% reduction in drag under identical conditions. This improvement is attributed to flow acceleration beneath the bow and the redistribution of pressure and viscous forces. However, this unusually large reduction reflects the idealized fixed-hull simulation conditions and far exceeds typical empirical improvements, indicating that caution is needed in interpreting these results. The results suggest that minor positive trim angles can substantially lower hydrodynamic resistance in this stepped planing hull configuration. Compared to prior studies, the magnitude of drag reduction observed here far exceeds reported values, largely because a simplified hull model is used at a high Froude number with the hull fixed in trim and heave.

1. Introduction

Leisure and performance segments depend largely on planing and increasingly on stepped-planing hulls. According to consolidated data from ICOMIA, Europe has approximately ten thousand marinas and more than one million wet berths. In the United States, the National Marine Manufacturers Association reports about eleven point eight million registered or documented boats and roughly three point six million unregistered craft, indicating a large and resilient user base for high-speed recreational vessels (European Boating Industry, 2023; NMMA, 2024a, 2024b). Against this backdrop, high speed craft design demands disciplined management of the speed range and weight while minimizing hydrodynamic resistance. With a study of designed spiral, classical planing formulations, most prominently the prismatic surface method, explain how increasing speed drives dynamic sinkage and wetted area growth, accelerating resistance at higher Froude numbers and clarifying the limits of displacement and stepless planing forms under fast craft conditions. These early-stage estimators remain valuable for sizing and screening; however, their simplifying assumptions motivate the need for complementary numerical or experimental assessments once trim, wetted area, and free-surface dynamics become tightly coupled (Savitsky, 1964; Vitiello et al., 2022).

A robust experimental–numerical corpus now underpins stepped-hull design. Towing-tank studies and RANS–VOF simulations consistently report resistance and trim gains when planing-specific meshing, interface-capturing, and turbulence-model choices are respected (De Marco et al., 2017; Pacuraru et al., 2022). Within this corpus, the Naples Systematic Series maps sensitivities to step number, height and longitudinal placement; transparent-bottom tests across approximately $Fr\nabla \approx 1.08–6.77$ visualize dry-area evolution and cavity behavior, while complementary works elucidate ventilation physics and appendage effects that further tune lift–drag and trim (Cucinotta et al., 2021; Vitiello et al., 2022; Yang et al., 2019). In parallel with this literature, recent methodological contributions on propulsion component matching for planing hulls and on CFD workflows for hydrodynamic form assessment provide additional background that it is drawn upon in the present study (Bayraktar et al., 2025; Göksu et al., 2024). Stepped planing hulls can exhibit complex flow phenomena that might be accentuated under fixed conditions. While Savitsky's classical method provides quick estimates for planing hull resistance, its simplifications and the lack of modern hull forms in its empirical basis justify the use of CFD for nuanced effects like trim influence on a stepped hull.

For compliance framing relevant to small craft, ISO 12215-5 uses a Froude-number-based criterion to determine whether a hull operates in a planing regime; this classification governs which load and scantling assumptions apply in design. Given the operating speed envelope examined here, our 10.60-m case hull satisfies the planing condition under ISO 12215-5's Froude-based approach, and power selection for recreational fast craft can subsequently be checked against the empirical maneuvering-speed method in ISO 11592-2 as a regulatory-aligned envelope alongside our Savitsky- and CFD-based estimates (ISO, 2019, 2021). Within this scope, the vessel examined in this study was constructed and validated through real sea trials. Notably, previous works have found only minor resistance reductions from optimal trim adjustments. This study explores a stepped-hull scenario at a considerably higher Froude number to examine whether a small trim angle can yield outsized effects, while recognizing that this approach is an idealized, fixed-trim analysis. A steady RANS CFD is employed to analyze a 10.6 m stepped planing hull at two trim settings while keeping the model fixed in position.

2. Material and Methodology

2.1. The Case Hull Model

The case vessel's particulars are detailed in Table 1, with an overall length of 10.60 meters and a length on waterline of 9.56 meters. A key indicator of its hydrodynamic performance is the block coefficient of 0.365. This relatively low value denotes a fine, typically associated with vessels designed for higher speeds or reduced resistance, rather than maximized carriage capacity.

Table 1. The key dimensions of the case ship

Particulars	Values	Units
Length overall (L_{oa})	10.60	m
Length on waterline (L_{wl})	9.56	m
Breadth (B)	3.04	m
Draught (amidships) (T)	0.60	m
Block coefficient (C_b)	0.365	--

The 3D model of the vessel was depicted in Fig. 1, visually confirms the main geometrical characteristic of the hull designed for high speeds and energy efficiency, aligning with its block coefficient value.

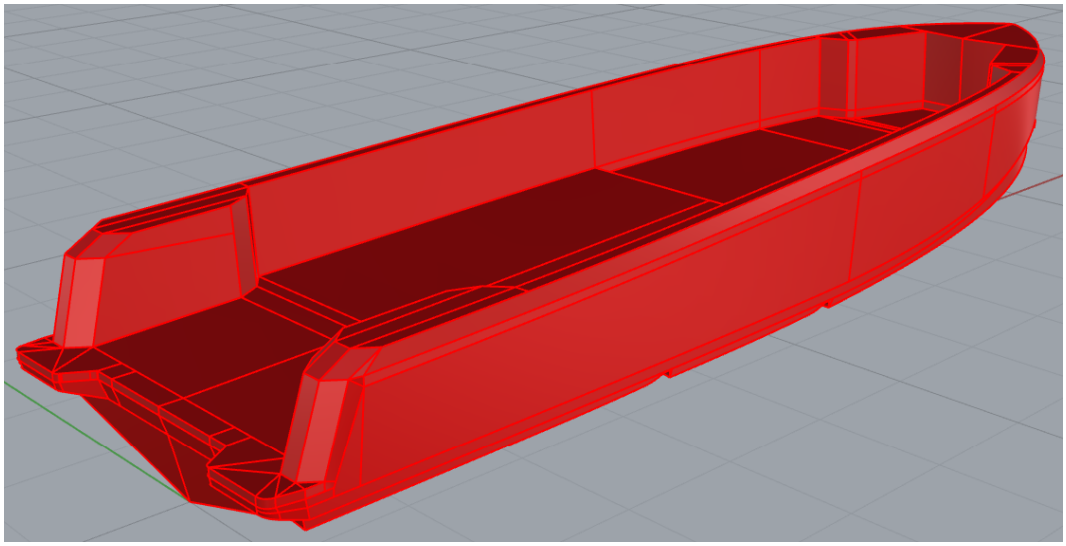

Fig. 1. The case planing hull model (Source: Authors' own work)

2.2. Resistance Prediction Methodologies

This section outlines the methods commonly employed in ship resistance analyses, including those used in this study. Prior to applying ship resistance analysis methods, it is essential to calculate the dimensionless Reynolds number to characterize the flow regime and evaluate the flow conditions (Deshpande et al., 2020). The primary difference between model- and ship-scale lies in the Reynolds number (Eq. 1), which reaches 10^6 in model-scale investigations and 10^9 at the ship-scale.

$$Re = \frac{\rho V L}{\mu} \tag{1}$$

ρ: density of fluid $[kg/m^3]$

V: ship or model speed $[m/s]$

L: characteristics length $[m]$

μ: dynamic viscosity $[Ns/m^2]$

The Froude number (Fr) is in Eq. (2) another critical dimensionless parameter in naval architecture and marine engineering, as it significantly influences ship resistance and performance (Terziev et al., 2021), where g represents the acceleration of gravity.

$$Fr = \frac{V}{\sqrt{gL}} \tag{2}$$

For the case hull of length L=10.60 m, at the simulation speed V=20.57 m·s^{-1}, the Reynolds number is approximately 2.17×10^8, and the Froude number is approximately 2.02, placing the vessel well within the high-speed planing regime.

2.2.1. Savitsky Method

A planing vessel can be differentiated from a normal displacement vessel by its method of weight support. It is important to note that, for a displacement vessel, the buoyancy force counterbalances its weight. A planing vessel sustains its weight by hydrodynamic lift forces produced while it navigates at high speed over water. When a planing vessel is stationary or moving at modest speeds, buoyancy sustains its weight. Consequently, when it accelerates, the hull design produces hydrodynamic lift forces that entirely sustain the hull. In certain watercraft, both lift and buoyancy provide support for the weight.

This article will present a theoretical method for assessing the performance of a planing boat (Savitsky, 1964), conducted several resistance experiments to establish the formula for the lift and drag of planing vessels, providing empirical relations for drag.

In this method, at equilibrium, a portion of the lift is produced by buoyancy, while the remainder is produced by hydrodynamic lift. The fundamental properties of the vessel are utilized as inputs, and the hull parameters are established. The metrics will thereafter be utilized to ascertain the vessel's resistance.

Despite its advantages, several limitations of the Savitsky method have been identified, particularly concerning the age of the empirical data underpinning the technique. The original dataset, derived from studies conducted in the 1960s and 1970s, may lack representation of modern hull designs and contemporary operational scenarios (Deng et al., 2021; Nikolopoulos & Boulougouris, 2019). Nevertheless, the method remains a valuable tool for resistance prediction during the early stages of ship design (Turan & Akman, 2021). It should be noted that the Savitsky method, while useful for initial estimates, does not directly account for stepped hull features or fixed-trim conditions examined in our CFD study. Thus, Savitsky's predictions are used as a baseline reference but rely on CFD for the detailed analysis.

2.2.2. Computational Fluid Dynamics Methodology

A vital numerical technique utilized in ship hydrodynamics is the solution of the Reynolds-Averaged Navier-Stokes (RANS) equations. The Navier-Stokes equations are essential for delineating fluid dynamics. Nonetheless, obtaining exact solutions to these equations is especially difficult in the context of turbulent flows. In the RANS equations, flow variables, including velocity and pressure, are represented as a time-averaged value augmented by a time-dependent turbulent component. Turbulent flows are frequently modelled using RANS equations, which are obtained from time-averaged calculations. Unsteady RANS simulations surpass the steady methodology, offering a more precise depiction of the temporal variations in turbulent flows. This study utilized the commercial CFD software program ANSYS Fluent as the RANS solver. The hull was rigidly fixed at the prescribed trim angle for each case. Two static trim conditions were simulated, a baseline of 0° and an elevated trim of 1.6°, with all other parameters identical.

Numerical simulations were conducted using ANSYS, a sophisticated commercial CFD software recognized for its effectiveness in solving complex fluid dynamics problems. The Steady RANS equations and the hull model were utilized to simulate the flow, yielding a steady state while accurately capturing the characteristics of the flow around the vessel. The Volume of Fluid (VOF) multiphase model was employed to accurately represent the dynamic interface between water and air. This method analyses the interface by computing a transport equation for the volumetric proportion of each fluid within each computational cell. The High-Resolution Interface Capturing (HRIC) technique was employed to improve accuracy in interface resolution, created in order to preserve an apparent interface, crucial for marine hydrodynamic simulations.

For the multiphase CFD analysis, the fluid properties were specified as follows: water was assigned a density of 998 kg.m-3 and a dynamic viscosity of 0.001003 Pa·s, while air was modelled with a density of 1.204 kg.m-3 and a dynamic viscosity of 1.813×10-5 Pa·s. The acceleration due to gravity was set to 9.81 m.s-2 to accurately account for gravitational forces influencing the fluid motion and free surface dynamics within the CFD simulations.

The boundaries of the computational area were meticulously defined to generate numerical computational domain by half of the hull model. A "velocity inlet" condition was implemented on the upstream and upper surfaces, guaranteeing a consistent and regulated fluid inflow, similar to a vessel motion in calm water condition. A "pressure outlet" condition was applied to the downstream surface, permitting fluid to escape the domain at atmospheric pressure, thereby simulating wake propagation. A "wall condition" was applied to the solid limits of the domain's side and bottom, enforcing the no-slip condition, which ensures that the fluid velocity at the wall corresponds with the wall's velocity. The ship's centerline was oriented on the midsection of the domain, that section also defined as symmetrical surface to mirror the fluid phenomena. Damping zones were established at both the inlet and outlet surfaces to mitigate the effects of wave reflections and to ensure precise movement of the free surface. Fig. 2 shows the computational domain, specifying the boundary conditions allocated to each surface together with their details, so presenting the numerical framework for the CFD analysis.

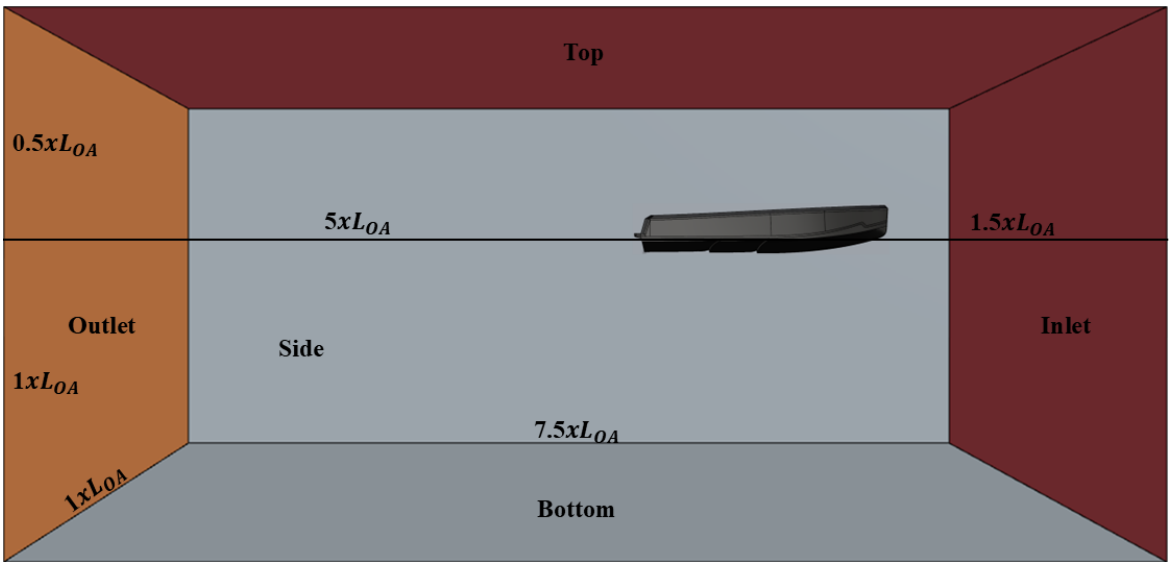

Fig. 2. Computational domain with specified boundary conditions and dimensions (Source: Authors' own work)

To enhance solution precision, three separate mesh refinement zones were meticulously created. These zones ensure high-resolution discretization in significant areas, facilitating exact viewing of free surface deformation and accurate resolution of essential wake formation details. Furthermore, background mesh refinement was employed in the static fluid domain to ensure precise and seamless transfer of computed flow properties between the presented hull grid and the stationary background grid, which is essential for maintaining numerical stability and accuracy throughout the simulation. Fig. 3 presents a comprehensive depiction of the mesh structure, emphasizing the implemented mesh and the distinct refinement zones, thereby elucidating the spatial discretization utilized for the CFD study.

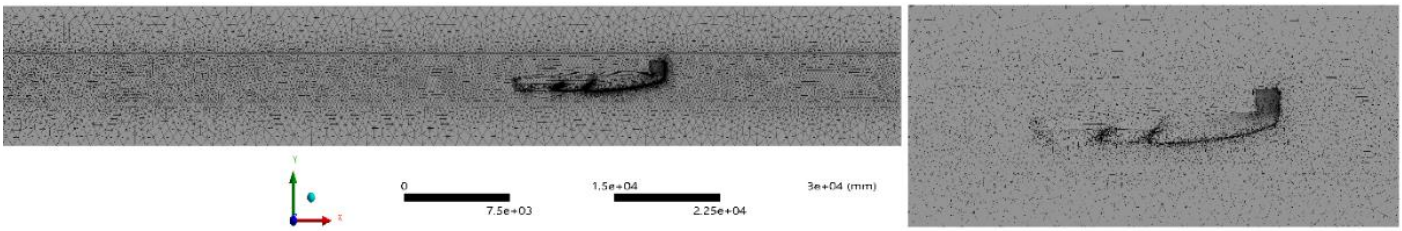

Fig. 3. The mesh structure and various details around mesh refinement zones (Source: Authors' own work)

The quality of the computational mesh is paramount for ensuring the accuracy and stability of the numerical solution. In this study, the generated mesh, comprising 3,572,223 elements and 641,522 nodes, was evaluated against stringent ANSYS quality metrics. The average Orthogonal Quality was remarkably high at 0.78909, placing it firmly within the "Very Good" range (0.70–0.95). Concurrently, the average Skewness value was only 0.20988, which falls into the "Excellent" category (0–0.25) (Cambaz et al., 2021; Gorgulu, 2024, 2025). To assess mesh adequacy, additional simulations were conducted using both a coarser and a finer mesh. The resulting drag forces varied within 3–5%, indicating sufficient grid independence for the current level of analysis. These metrics confirm that the mesh exhibits excellent geometric integrity, minimizing potential numerical diffusion and solver instability. Such high-quality meshing is critical, as it provides a robust foundation for the CFD simulations, thereby increasing confidence in the reliability and physical fidelity of the final results. The accuracy of turbulent flow simulations, particularly in the near-wall region, fundamentally depends on the resolution of the computational mesh, as indicated by the dimensionless wall distance, y^+. This parameter defines the height of the first cell center from the wall in viscous units, which is critical for determining the appropriate near-wall treatment method for the chosen turbulence model. The SST k–w turbulence model was employed for its proven accuracy in ship hydrodynamics, with near-wall refinement targeting y^+ in the appropriate range for either low-Reynolds modeling or wall functions as needed. The target y^+ value is typically established prior to meshing to ensure that the initial computational cell is positioned within a specified region of the turbulent boundary layer, thereby influencing the resolution of the boundary layer or its representation via wall functions. Selecting an

appropriate y^+ value is essential for accurate predictions of wall shear stress, drag, and flow separation. This choice is often validated through post-processing to confirm that the mesh resolution adequately represents the intricate flow phenomena adjacent to solid surfaces. Friction velocity, non-dimensional wall velocity and non-dimensional wall distance are given in Equations 3-5.

Friction velocity (u^*):

$$u^* = \sqrt{\frac{T_w}{\rho}} \tag{3}$$

Non-dimensional wall velocity (u^+):

$$u^+ = \frac{u}{u^*} \tag{4}$$

Non-dimensional wall distance (y^+):

$$y^+ = \frac{\rho u^*}{\mu} y \tag{5}$$

where, T_w is the skin friction, u is the local velocity, μ is the dynamic viscosity of the fluid, and y is for the wall-normal coordinate.

Hydrodynamic forces were computed by integrating pressure and shear stress on the hull. In post-processing total resistance is obtained for each case; this can be further decomposed into viscous and pressure drag components. In the present study, the study focused on total drag for the comparison, but the methodology allows examination of each component separately.

3. Results and Discussion

Fig. 4. illustrates the velocity and turbulence kinetic energy contours for the hull models without trim (a, c) and with a 1.6° trim angle (b, d). The quantitative comparison demonstrates that the introduction of a trim angle significantly modifies both the flow field and turbulence characteristics around the hull. In the non-trimmed configuration, the maximum velocity magnitude in the flow domain reaches approximately 20.8 $m \cdot s^{-1}$, with an average velocity near the hull surface of 17.0 $m \cdot s^{-1}$. The flow remains relatively uniform, and only a narrow wake region forms behind the stern, where the velocity decreases to about 6–8 $m \cdot s^{-1}$. This stable flow separation indicates efficient momentum recovery in the aft region, suggesting a balanced pressure distribution and limited drag contribution from wake turbulence.

In contrast, when a 1.6° trim angle is applied, the maximum velocity increases slightly to 20.6 $m \cdot s^{-1}$, but the acceleration of the flow near the hull bottom becomes more distinct. The region of elevated velocity extends further downstream, while the average near-surface velocity decreases to 15–16 $m \cdot s^{-1}$ due to the altered incidence of the flow. This redistribution of velocity gradients implies a local reduction in hydrodynamic lift near the stern and a corresponding increase at the bow, producing a measurable shift in the hydrodynamic balance. The turbulence kinetic energy (TKE) results reveal a similar trend. In the non-trimmed hull, the TKE remains below 18 $m^2 \cdot s^{-2}$, concentrated in a confined region just behind the stern. The 1.6° trimmed hull, however, exhibits a notable reduction in overall TKE intensity, with maximum values around 9.6 $m^2 \cdot s^{-2}$. Despite this decrease in peak magnitude, the turbulent region expands longitudinally, indicating a more extended but less intense wake. This behavior suggests that while the local turbulence generation decreases, the wake persistence increases, which may affect the total resistance distribution between pressure and viscous components. The combined interpretation of velocity and turbulence fields indicates that the trim angle induces a trade-off between flow acceleration and wake expansion. Such modifications directly influence the total drag experienced by the hull.

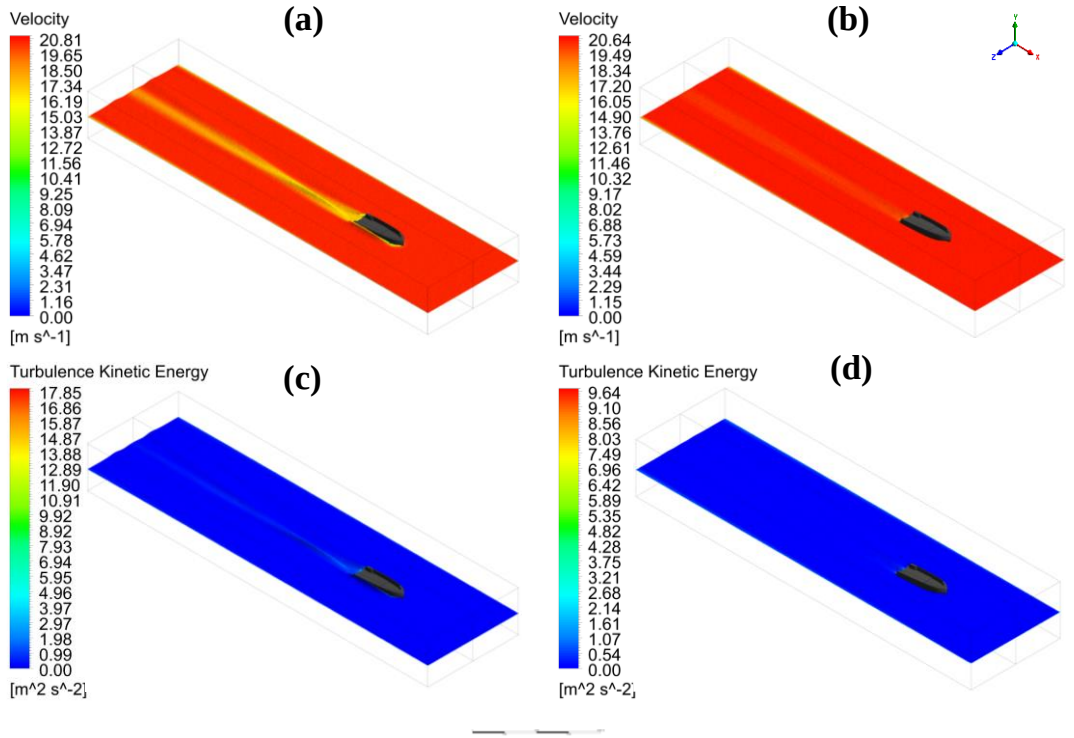

Fig. 4. Velocity (a–b) and turbulence kinetic energy (c–d) contours for hulls without trim (a, c) and with 1.6° trim (b, d) (Source: Authors' own work)

The integrated drag force for the hull without trim is 22592.89 N, while the 1.6° trimmed hull yields 3009.294 N under identical operating conditions. This magnitude of reduction is exceptionally high and not seen in prior experimental or numerical studies. It likely results from the specific conditions of our simulation, notably the fixed hull position and the chosen trim angle being near an optimal point, rather than indicating a generally achievable improvement. The trim therefore reduces drag by 86.68% relative to the baseline, corresponding to a reduction factor of 7.5×. This reduction aligns with the observed shift in the velocity field and the concurrent decrease in peak TKE, indicating that trim-induced flow acceleration underneath the bow and the lengthened but milder wake collectively lower the net resistance. The results indicate that a small positive trim can produce a substantial reduction in hydrodynamic resistance by rebalancing pressure and viscous contributions through controlled flow acceleration and moderated wake intensity. A sensitivity analysis over neighboring trim angles would clarify whether 1.6° lies near a local optimum for minimum resistance. It should be noted that a real planing hull at Fr approximately 2 would not remain at 0◦ trim; it would naturally trim up and rise due to hydrodynamic lift. In the baseline CFD case, the hull was artificially held at 0◦, likely causing an excessive wetted surface and higher drag than a free-trimming hull would experience at this speed. Thus, when the hull is trimmed to 1.6° in the simulation, it is moved closer to the hull's favorable running attitude, resulting in a dramatic drop in drag. In reality, the boat would have already adopted some positive trim, so the incremental benefit of 1.6° additional trim would be much smaller. To better understand the nature of the drag reduction, it is considered the two main components of resistance. The CFD simulation's output can be separated into frictional drag and pressure drag. In high-speed planing conditions, frictional drag typically constitutes a large fraction of total resistance. The introduction of a positive trim likely reduced the wetted area significantly, thereby lowering frictional resistance. Meanwhile, the pressure drag would also change: at 1.6° trim the pressure distribution shifts, which can reduce form drag as well. Based on prior studies, the frictional component is expected to dominate; for instance, Le et al. observed an 8% reduction in pressure drag but only 1.5% in total drag when optimizing trim, implying that viscous resistance was the larger portion. In this case, the majority of the 86% total drag reduction is therefore likely attributable to a drop in viscous drag due to less wetted surface at the higher trim (Le et al., 2021). The pressure drag component would have decreased to a lesser extent, consistent with the more moderate changes in wake pressure field observed.

The findings of this study were compared with previous numerical and experimental investigations to evaluate their consistency and to highlight the distinct behavior of the present hull configuration. Le et al. conducted a

numerical analysis of the US Navy Combatant DTMB 5415 model and reported that optimal trim and draft conditions resulted in approximately 1.5 % reduction in total resistance and up to 8 % reduction in pressure drag (Le et al., 2021). Similarly, Martić et al. investigated the effect of trim under various operating conditions and found that moderate trim angles could decrease total resistance by 1.5–3 % depending on the Froude number and hull form (Martić et al., 2024). In contrast, Sherbaz and Duan observed that certain trim configurations, particularly bow-down conditions, could increase total resistance due to enhanced flow separation and stern turbulence (Sherbaz & Duan, 2014). The contrast between the literature and these result underscores that this scenario is highly specific. It combines a simplified geometry, a fixed high trim at speed, and a possibly optimal configuration, conditions under which the CFD solver predicts an outsized effect. Such conditions are unlikely to be fully realized in practice, which is why prior experimental studies have not reported anything comparable. Even classical semi-empirical methods would predict far smaller changes for a 1–2° trim variation, although those methods don't capture step effects (Savitsky, 1964).

Compared with these studies, the present analysis demonstrated a substantially higher drag reduction of 86.68 % when a 1.6° trim angle was applied. This deviation from the typical literature can be attributed to several factors. First, the current model represents a simplified and smaller-scale hull with a fixed free-surface height and limited degrees of freedom, which amplifies the relative impact of geometric inclination. Second, the analysis was performed at a constant inlet velocity of 20.57 $m \cdot s^{-1}$, significantly higher than those used in conventional ship resistance experiments. Third, only two conditions which are zero trim and 1.6° trim were considered, and the selected angle may coincide with a local optimum for minimum resistance in this specific configuration. Because it is simulated only two trim states, it is unclear whether the relationship between trim angle and resistance is smooth or if 1.6° happens to be near an optimal point. A finer sweep of trim angles would be needed to map out the resistance curve, it is quite possible that 1.6° lies close to a minimum-resistance trim, which made the two-point comparison seem especially dramatic. Future work will investigate intermediate trim values to confirm the trend. In the non-trimmed configuration, the maximum flow velocity reaches approximately 20.8 m.s-1 and averages approximately 17.0 m.s-1 near the hull. Only a narrow wake region forms behind the stern, indicating efficient momentum recovery and limited wake turbulence. In contrast, with a 1.6° trim, the peak velocity is similar but flow acceleration near the hull bottom is more pronounced, and the high-velocity region extends further aft. The near-surface velocity averages a lower 15–16 m.s-1 due to the flow's altered incidence on the hull.

4. Conclusions

The computational fluid dynamics analysis demonstrated that adjusting the trim angle has a significant influence on the hydrodynamic performance of stepped planing hulls. A positive trim angle of 1.6° changed the pressure distribution and wake structure, resulting in a large reduction in both drag and turbulence intensity. The total drag decreased from 22,592.89 N to 3,009.294 N, representing an 86.68% reduction in resistance under these simulation conditions. The turbulence kinetic energy decreased from 18 $m^2 \cdot s^{-2}$ to 9.6 $m^2 \cdot s^{-2}$, indicating reduced flow instability and improved wake recovery. Compared with previously reported experimental and numerical results, which typically indicate a reduction of 1 to 10 percent, the drag decrease obtained in this analysis is considerably higher. This outlier result is explained by the simplified hull geometry, fixed high-speed input, and the absence of dynamic trim/heave in the model. In other words, the simulation likely over-predicts the benefit of a small trim adjustment. Real-world improvements would be expected to be much smaller, as indicated by previous studies. This difference can be explained by the simplified hull geometry, the fixed inlet velocity of 20.57 $m \cdot s^{-1}$, and the restricted motion of the numerical model. Nevertheless, the flow pattern observed in this study, characterized by accelerated flow beneath the bow and a longer but weaker wake, remains consistent with established hydrodynamic principles. Because these CFD findings have not yet been validated against experiments or established empirical methods, they should be viewed as preliminary. Conducting towing tank experiments on the same hull would help verify the accuracy of the predicted forces. Indeed, validation through measurements is essential to determine how much of the 86% drag reduction would materialize in practice.

Further studies should include a more detailed mesh structure to improve the resolution of flow gradients near the hull surface and the free surface. It is also recommended to examine several trim angles and a wider range of Froude numbers to identify the optimum condition for minimum drag. In addition, modifying the geometry of the step hull, including the position and height of the step, may provide valuable insights into how hull form affects resistance and wake development. Finally, validation through experimental measurements in a towing tank would increase the reliability of the numerical findings and support future optimization studies on stepped planing hulls.

Acknowledgements

The authors would like to express their sincere appreciation to Mert Tepe, Industrial and Product Designer, for sharing valuable insights and for granting permission to utilize the information provided during the study.

References

Bayraktar, M., Göksu, B., & Yüksel, O. (2025). Matching of propulsion system components for a planing hull model. *Ships and Offshore Structures*, 20(6), 755–766. https://doi.org/10.1080/17445302.2024.2356949

Cambaz, A., Görgülü, Y. F., & Arat, H. (2021). Two-Phase Numerical Modelling of a Wet Exhaust System in a Catamaran Motor Yacht Diesel Engine. *European Journal of Science and Technology*, (31), 165–170. https://doi.org/10.31590/ejosat.1007351

Cucinotta, F., Mancini, D., Sfravara, F., & Tamburrino, F. (2021). The Effect of Longitudinal Rails on an Air Cavity Stepped Planing Hull. *Journal of Marine Science and Engineering*, 9(5), Article 470. https://doi.org/10.3390/jmse9050470

De Marco, A., Mancini, S., Miranda, S., Scognamiglio, R., & Vitiello, L. (2017). Experimental and numerical hydrodynamic analysis of a stepped planing hull. *Applied Ocean Research*, 64, 135–154. https://doi.org/10.1016/j.apor.2017.02.004

Deng, R., Wang, S., Hu, Y., Wang, Y., & Wu, T. (2021). The effect of hull form parameters on the hydrodynamic performance of a bulk carrier. *Journal of Marine Science and Engineering*, 9(4), Article 373. https://doi.org/10.3390/jmse9040373

Deshpande, S., Sundsbø, P., & Das, S. (2020). Ship resistance analysis using CFD simulations in Flow-3D. *International Journal of Multiphysics*, 14(3), 227–236. https://doi.org/10.21152/1750-9548.14.3.227

European Boating Industry. (2023). *Facts & Figures*. https://www.europeanboatingindustry.eu/about-the-industry/facts-and-figures

Göksu, B., Erginer, K. E., & Öner, G. (2024). Comparison of submarine hull morphologies obtained by biomimicry method with DARPA SUBOFF. *Naval Engineers Journal*, 136(3), 87–104.

Gorgulu, Y. F. (2024). Thermal efficiency evaluation in shell-and-tube heat exchangers: A CFD-based parametric study. *Proceedings of the Institution of Mechanical Engineers, Part E: Journal of Process Mechanical Engineering*. 240(2). https://doi.org/10.1177/09544089241262481

Gorgulu, Y. F. (2025). CFD-based cooling performance of gas turbine blades. *Aircraft Engineering and Aerospace Technology: An International Journal*, 98(2), 154-168. https://doi.org/10.1108/AEAT-01-2025-0037

ISO. (2019). *ISO (2019/2025) ISO 12215-5: Small craft—Hull construction and scantlings*. https://www.iso.org/standard/69552.html

ISO. (2021). *ISO (2021) ISO 11592-2: Small craft—Determination of maximum propulsion power rating using manoeuvring speed*. https://www.iso.org/standard/81925.html

Le, T.-H., Vu, M. T., Bich, V. N., Phuong, N. K., Ha, N. T. H., Chuan, T. Q., & Tu, T. N. (2021). Numerical investigation on the effect of trim on ship resistance by RANSE method. *Applied Ocean Research*, 111, Article 102642. https://doi.org/10.1016/j.apor.2021.102642

Martić, I., Anušić, B., Degiuli, N., & Grlj, C. G. (2024). Numerically Investigating the Effect of Trim on the Resistance of a Container Ship in Confined and Shallow Water. *Applied Sciences*, 14(15), Article 6570. https://doi.org/10.3390/app14156570

Nikolopoulos, L., & Boulougouris, E. (2019). A study on the statistical calibration of the holtrop and Mennen approximate power prediction method for full hull form, low froude number vessels. *Journal of Ship Production and Design*, 35(1), 41–68. https://doi.org/10.5957/JSPD.170034

NMMA. (2024a). *2023 Total Boat Registrations Report Highlights Trends in Boat Use*. https://www.nmma.org/press/article/24858

NMMA. (2024b). *U.S. Recreational Boating Statistical Abstract*. https://www.nmma.org/statistics/publications/statistical-abstract

Pacuraru, F., Mandru, A., & Bekhit, A. (2022). CFD Study on Hydrodynamic Performances of a Planing Hull. *Journal of Marine Science and Engineering*, 10(10), Article 1523. https://doi.org/10.3390/jmse10101523

Savitsky, D. (1964). Hydrodynamic Design of Planing Hulls. *Marine Technology and SNAME News*, 1(04), 71–95. https://doi.org/10.5957/mt1.1964.1.4.71

Sherbaz, S., & Duan, W. (2014). Ship Trim Optimization: Assessment of Influence of Trim on Resistance of MOERI Container Ship. *The Scientific World Journal*, 2014, Article 03695. https://doi.org/10.1155/2014/603695

Terziev, M., Tezdogan, T., Demirel, Y. K., Villa, D., Mizzi, S., & Incecik, A. (2021). Exploring the effects of speed and scale on a ship's form factor using CFD. *International Journal of Naval Architecture and Ocean Engineering*, 13, 147–162. https://doi.org/10.1016/j.ijnaoe.2020.12.002

Turan, B. İ., & Akman, M. (2021). Modeling and Comparison of Bodrum Gulets' Hull Forms with Round and Transom Sterns. *Journal of Eta Maritime Science*, 9(2), 120–129. https://doi.org/10.4274/jems.2021.09327

Vitiello, L., Mancini, S., Bilandi, R. N., Dashtimanesh, A., De Luca, F., & Nappo, V. (2022). A comprehensive stepped planing hull systematic series: Part 1 - Resistance test. *Ocean Engineering*, 266, Article 112242. https://doi.org/10.1016/j.oceaneng.2022.112242

Yang, D., Sun, Z., Jiang, Y., & Gao, Z. (2019). A Study on the Air Cavity under a Stepped Planing Hull. *Journal of Marine Science and Engineering*, 7(12), Article 468. https://doi.org/10.3390/jmse7120468